



1 **Impact of Eurasian autumn snow on the winter North Atlantic**
2 **Oscillation in seasonal forecasts of the 20th century.**

3

4 Martin Wegmann^{1,2,3}, Yvan Orsolini⁴, Antje Weisheimer^{5,6}, Bart van den Hurk^{6,7} and Gerrit
5 Lohmann³

6

7 ¹Institute of Geography, University of Bern, Bern, Switzerland.

8 ²Oeschger Centre for Climate Change Research, University of Bern, Bern, Switzerland.

9 ³Alfred-Wegener-Institute, Helmholtz Center for Polar and Marine Research, Bremerhaven, Germany

10 ⁴NILU–Norwegian Institute for Air Research, Kjeller, Norway

11 ⁵National Centre for Atmospheric Science, Atmospheric, Oceanic and Planetary Physics, University of
12 Oxford, Oxford, United Kingdom

13 ⁶European Centre for Medium-Range Weather Forecasts, Reading, United Kingdom

14 ⁷Deltares, Delft, The Netherlands

15

16

17 Corresponding author: Martin Wegmann, Institute of Geography and Oeschger Centre for Climate
18 Change Research, University of Bern, Hallerstrasse 12, 3012 Bern, Switzerland. Email:
19 martin.wegmann@giub.unibe.ch

20

21 **Key points**

22 Snow–atmosphere coupling, seasonal prediction, North Atlantic Oscillation, polar vortex, stratospheric
23 warming, hindcast

24



25 **Abstract**

26 As the leading climate mode of wintertime climate variability over Europe, the North Atlantic
27 Oscillation (NAO) has been extensively studied over the last decades. Recently, studies highlighted the
28 state of the Eurasian cryosphere as a possible predictor for the wintertime NAO. However, missing
29 correlation between snow cover and wintertime NAO in climate model experiments and strong non-
30 stationarity of this link in reanalysis data is questioning the causality of this relationship.

31 Here we use the large ensemble of Atmospheric Seasonal Forecasts of the 20th Century (ASF-20C)
32 with the European Centre for Medium-Range Weather Forecasts model, focusing on the winter season.
33 Besides the main 110-year ensemble of 51 members, we investigate a second, perturbed ensemble of
34 21 members where initial (November) land conditions over the Northern Hemisphere are swapped from
35 neighboring years. The Eurasian snow / NAO linkage is examined in terms of a longitudinal snow depth
36 dipole across Eurasia. Subsampling the perturbed forecast ensemble and contrasting members with high
37 and low initial snow dipole conditions, we found that their composite difference indicates more negative
38 NAO states in the following winter (DJF) after positive west to east snow cover gradients at the
39 beginning of November. Surface and atmospheric forecast anomalies through the troposphere and
40 stratosphere associated with the anomalous positive snow dipole consist of colder early winter surface
41 temperatures over Eastern Eurasia, an enhanced Ural ridge and increased vertical energy fluxes into the
42 stratosphere, with a subsequent negative NAO-like signature in the troposphere. We thus confirm the
43 existence of a causal connection between autumn snow patterns and subsequent winter circulation in
44 the ASF-20C forecasting system.



45 **1. Introduction**

46 As the leading climate variability pattern affecting winter climate over Europe, the North Atlantic
47 Oscillation (NAO) has been extensively studied over the last decades (Wanner et al., 2001; Hurrell and
48 Deser, 2010; Moore and Renfrew, 2012; Deser et al., 2017). The NAO state strongly impacts the
49 hydroclimate as well as the ecological and socioeconomic conditions over major population clusters of
50 Europe and North America. In its positive state, the NAO projects onto strong pressure gradients over
51 the North Atlantic, strong westerly winds and mild but wet conditions for Central Europe. A negative
52 winter NAO is connected to a southwardly displaced Atlantic jet stream, weaker westerlies and cold,
53 dry conditions for Central Europe. The NAO also shows a distinct quadrupole signature in surface
54 temperature straddling the Atlantic, with two opposite poles over northern Europe and Greenland
55 /Labrador and an opposite pair further south over southern Europe/North Africa and the US East Coast.
56 Recent cases of extreme negative NAO states (Wang and Chen, 2010; Lü et al., 2020), including the
57 winter 2020/2021, coincided with several extreme weather events across the Northern Hemisphere,
58 including cold air outbreaks with record snowfall at locations over Southern and Northern Europe, as
59 well as eastern parts of Canada and the United States.

60 Improving seasonal to decadal predictions of the winter NAO is a high-priority research for many
61 weather and climate related research centres (Kang et al., 2014; Scaife et al., 2014, 2016; Smith et al.,
62 2016; Dunstone et al., 2016; Athanasiadis et al., 2017; Weisheimer et al., 2017; Baker et al., 2018;
63 Weisheimer et al., 2019). Despite its stochastic behaviour, the NAO state was shown to be modulated
64 by slowly varying components of the climate system, carrying climate state „memory“ across months
65 or even seasons (Dobrynin et al., 2018; Meehl et al., 2021). Initially discussed by Cohen and Entekhabi
66 (1999), recent studies have highlighted the potential of Eurasian autumn snow cover anomalies as a
67 useful predictor for the boreal wintertime (December– January–February, DJF) NAO in empirical
68 prediction models (Cohen et al., 2007, 2014; Cohen and Jones 2011; Peings et al., 2013; Tian and Fan
69 2015; Wang et al., 2017; Han and Sun 2018; Wegmann et al., 2020).

70 The causal chain behind the snow impact is hypothesized as follows: due to the radiative and
71 thermodynamical properties of snow (Cohen and Rind 1991; Vavrus 2007; Dutra et al., 2011;
72 Thackeray et al., 2019), a thicker and more extended snowpack is associated with coherent surface
73 cooling. Cohen et al., (2007; see also Cohen et al., 2014; Henderson et al., 2018 for reviews) proposed
74 a multi-step mechanism whereby this surface cooling leads to raised isentropic surfaces, triggering
75 increased Rossby wave activity propagating upward and being absorbed in the stratosphere, warming
76 it and subsequently weakening the polar vortex. The negative stratospheric Northern Annular Mode
77 (NAM) signal eventually propagates down into the troposphere and to the surface where it projects onto
78 a negative NAO.

79 Investigating the robustness of this mechanism is challenged by several elements. Observational studies
80 analyzing statistical links are restricted by the relatively short length (a few decades) of comprehensive



81 and complete snow cover observations. Using long-term reanalyses, recent studies showed substantial
82 non-stationary relationships between autumn Eurasian snow cover and the sign of the winter NAO over
83 the span of the 20th century (Peings et al., 2013; Douville et al., 2016; Wegmann et al., 2020). Using
84 shorter time scales, the probability of “cherry picking” a period of increased correlation and sampling
85 co-variability with other climate system components increases considerably. Causes for the non-
86 stationarity are still discussed, with possible influences from the Quasi-Biennial Oscillation (QBO), El
87 Niño-Southern Oscillation (ENSO) or simply snow cover variance (Peings et al., 2017; O’Reilly et al.,
88 2017; Tyrrell et al., 2018; Wegmann et al., 2020; Weisheimer et al., 2020). Disentangling co-variability
89 is further challenged by the co-occurrence of increased Eurasian snow cover and increased Ural
90 blocking frequency, questioning the lead-lag relationship between snow cover and blocking (Peings
91 2019; Song and Wu, 2019; Santolaria-Otín et al., 2021). Moreover, a variety of temporal and spatial
92 snow cover indices used among the different studies obstruct direct comparisons. Nevertheless, recent
93 studies point out that a November longitudinal snow cover dipole across Eurasia shows the strongest
94 statistical link to the DJF NAO state (Gastineau et al., 2017; Han and Sun 2018; Santolaria-Otín et al.,
95 2021).

96 Analyzing the snow → NAO mechanism in modelling experiments is challenged by short-comings of
97 the current Atmospheric or Atmosphere-Ocean General Circulation Models (AGCMs or AOGCMs)
98 regarding snow-atmosphere feedbacks (Santolaria-Otín and Zolina 2020). Most of the free-running
99 Coupled-Model Intercomparison Project (CMIP) models do not capture the statistical snow-NAO link
100 found in reanalyses data (Hardimann et al., 2008; Furtado et al., 2015; Gastineau et al., 2017). On the
101 other hand, when large snowpack anomalies are prescribed through nudging or imposed as initial
102 conditions, several AGCM experiments showed promising results for identifying several to all steps of
103 the proposed mechanism (Gong et al., 2003; Fletcher et al., 2009; Peings et al., 2012; Tyrrell et al.,
104 2018).

105 Some of the current-generation subseasonal-to-seasonal or seasonal coupled prediction models also
106 seem to catch parts of the mechanism chain, specifically negative temperature anomalies associated
107 with a thicker snowpack (Orsolini et al., 2013; Diro and Lin, 2020) as well as an enhanced wave activity
108 generating upward fluxes into the stratosphere associated with ridging over western or eastern Eurasia
109 (Orsolini et al., 2016; Li et al., 2019; Garfinkel et al., 2020), although several models failed to simulate
110 that ridging in the latter multi-model study. The subsequent stratosphere-troposphere coupling
111 influencing the surface Arctic Oscillation also tended to be weak to non-existent in most models. These
112 studies have been limited to the recent decades and, consequently, confidence in the robustness of the
113 mechanism across spans of decades is still low and needs to be strengthened (Garfinkel et al., 2020).

114 To disentangle the issues of non-stationarity (found in observations) and causality (found in models),
115 we base our investigation on a 110-year long (1901-2010) ensemble seasonal prediction experiment,
116 which is based on the historical seasonal forecast initiative using ECMWF’s atmosphere-only model,



117 called “ASF-20C” (Weisheimer et al., 2017). This 51-member ensemble experiment with four start
118 dates per year and a forecast length of 4 months has been used in several studies on the predictability
119 of the NAO and other climate patterns (e.g., O’Reilly et al., 2017; Parker et al., 2019; Weisheimer et
120 al., 2019; Weisheimer et al., 2020; O’Reilly et al., 2020). To investigate the influence of land surface
121 conditions, in this case snow cover, on the evolution of the atmospheric state throughout the season, we
122 use a novel, 21-member twin set of the ASF-20C forecasts with perturbed initial land conditions. This
123 dataset was used as a pilot experiment in the context of the Land Surface, Snow and Soil moisture
124 Model Intercomparison Program LS3MIP (Van den Hurk et al., 2016), aimed at reproducing land
125 surface potential predictability experiments as described by Dirmeyer et al. (2013). We aim to address
126 the question of causality, pathway, stationarity and seasonal evolution of the proposed mechanism of
127 the snow-stratosphere-troposphere linkage over decadal to centennial time scales.

128 This paper is organized as follows. Sect. 2 describes the data and methods used. In Sect. 3, we show
129 winter evolution of climate anomalies for the different initialization runs and contrast them with
130 observed anomalies. The results are discussed in Sect. 4 and finally summarized in Sect. 5.

131



132 2. Data and Methods

133 a. Climate reanalysis and reconstruction

134 We use the Centre for Medium-Range Weather Forecasts (ECMWF) product ERA-20C (ERA20C; Poli
135 et al., 2016) to investigate pre-conditions and the initialization of the seasonal predictions, to compute
136 the DJF NAO index as well as to create a Eurasian snow dipole index. ERA-20C only assimilates
137 surface pressure and marine wind observations, with sea surface temperature (SSTs) boundary
138 conditions taken from the HadISST2.1.0.0 datasets (Rayner et al., 2003). ERA-20C was found to
139 represent interannual snow variations over Eurasia remarkably well. For an in-depth discussion of its
140 performance and the technical details concerning snow computation, see Wegmann et al., (2017). Due
141 to the a-forementioned statistical impact for the winter NAO evolution, we focus on the November
142 Eurasian snow dipole index as predictor for the following NAO state (Gastineau et al., 2017; Han and
143 Sun 2018; Santolaria-Otín et al., 2021). Following Han and Sun (2018), we calculate the index over the
144 period 1901–2010 by averaging snow depths over the western domain (30°–60°E, 48°N–58°N) and the
145 eastern domain (80°–130°E, 40°–56°N), eventually subtracting the western domain from the eastern
146 domain to derive the west-east snow cover gradient. Hence, a positive snow index indicates higher snow
147 depths in the eastern domain and a positive longitudinal snow gradient. The index is normalized and
148 linearly detrended with respect to the overall time period. To comply with the initialization date of 1st
149 of November for the seasonal prediction runs, we calculate the index for 1st of November instead of
150 November mean snow (Figure 1). Even though Han and Sun (2018) calculated the dipole index using
151 snow cover, we used snow depth since ERA-20C provides snow depth as the actual prognostic variable.
152 We hence refrained from using empirical rules to convert snow depth to snow cover. We found the
153 index based on snow depth to be virtually identically (also see Supplementary Figure S1) to the index
154 using snow cover (see also Wegmann et al., 2020 for more insights).

155 To compute the winter NAO index, we normalize the first Empirical Orthogonal Function of ERA-20C
156 DJF sea level pressure (SLP) for the region (90°–50°E, 20°–80°N). We use the same definition for the
157 NAO DJF index in seasonal prediction runs and compare those with the reconstructed, independent DJF
158 NAO index by Jones et al., (1997) from the Climate Research Unit (CRU).

159 b. Seasonal prediction experiments

160 Additionally, we use atmospheric seasonal retrospective predictions covering the 110-year period 1901-
161 2010 of ERA-20C with 51 ensemble members of the ASF-20C hindcasts (hereafter ASF-20C CTL)
162 (Weisheimer et al., 2017). The atmospheric model used for the 4-month forecasts is the ECMWF
163 Integrated Forecast System Version CY41R1 and is initialized at four start dates per year (1st of Feb,
164 May, Aug and Nov) with ERA20C land and atmospheric conditions. It uses the same lower boundary
165 conditions for SST and sea ice as ERA-20C. Here, we only use forecasts initialized on the 1st of
166 November. The horizontal spectral resolution of the model of T255 is similar to ECMWF's previous
167 operational system System 4 (Molteni et al., 2011) and corresponds to a grid length of approximately



168 80 km. The model has 91 vertical levels and a top at 0.01 hPa. The ensemble has been created by
169 perturbing each member through the stochastic physics schemes to represent model uncertainties in a
170 similar way as the a-forementioned System 4.

171 To investigate the impact of Eurasian snow depth we use an additional set of perturbed forecasts, based
172 on a 21-member subset of the ASF-20C CTL experiment (hereafter, the “Experiment” or ASF-20C
173 EXP). Each member run is initialized with different land surface conditions, sampled from the
174 neighbouring 20 years. For example, the range of land surface conditions for the 21-member ensemble
175 forecast initialised on 1st of November 1950 spans the land surface conditions of the years 1940–1960:
176 member 01 is initialized with the land surface conditions of 1940, member 02 of 1941, member 03 of
177 1942 and so forth. For the beginning and ending ten years of the hindcast dataset, the land surface
178 conditions are sampled from the closest 21 neighbouring years within the dataset. Here, land surface
179 conditions include the entire land state, including soil moisture, snow depth and soil temperatures. We
180 argue that for investigating northern hemisphere climate anomalies of the 1st of November initialization,
181 snow depth has by far the largest impact on atmospheric dynamics compared to soil moisture and soil
182 temperatures, thus allowing us to attribute the differences to snow changes. The main bulk of the
183 experiment data has a monthly resolution, daily data is only available for selected variables and three
184 tropospheric levels.

185 Taking advantage of the shuffled initial land conditions of ensemble members in ASF-20C EXP, we
186 subsample members with positive or negative initial Eurasian snow dipole (Figure 2). This conditional
187 sampling approach has been used when testing the sensitivity of extended range forecasts to soil
188 moisture (Koster et al., 2011; van den Hurk et al., 2012) or to snow initial conditions (Li et al., 2019;
189 Garfinkel et al., 2020). For each start date, we can identify those members with positive or negative
190 initial snow dipole indices, corresponding to different years of the shuffled land initialisation. We
191 further proceed with compositing these two selected sets. Due to the decadal variability in the November
192 snow cover, the amount of “high snow members” (positive dipole index) and “low snow members”
193 (negative dipole index) varies throughout the 110 years. There might be periods when a majority of the
194 neighbouring 20 years shows a positive snow dipole index and other periods when a minority does. To
195 avoid this variation of the composited ensemble size across the years, we only use the five ensemble
196 members with the most positive and most negative initial Eurasian snow dipole, creating two ensemble
197 means (each of size N=5), namely a high snow dipole ensemble-mean and low snow dipole ensemble
198 mean, for each winter through the 110-year period.

199 It should be noted that the absolute magnitude of the ensemble-mean snow differences is still changing
200 from year to year. For example, the most positive snow dipole for the period 1910–1930 might be lower
201 than in the time window 1980–2000, and the same applies for negative dipole indices. Due to the
202 definition of the ASF-20C EXP, this setup is unavoidable, but it also allows for realistic magnitudes of



203 snow forcings and for incorporating a realistic natural variability into the experiment. The (5-member)
204 ensemble-mean difference (Figure 3a) displays a snow depth increase of 1-2 cm over Central and
205 Eastern Siberia, together with a 0.2-1 cm snow depth decrease over Western Russia, as expected from
206 the snow dipole definition. Concomitant negative anomalies (1-2 cm snow depth) nevertheless extend
207 outside of the dipole definition domains to more northern latitudes, e.g., over Western Russia and the
208 Russian Far East, or over the coastal mountain ranges of the North American Pacific Northwest. Note
209 that these two domains are in snow transition zones, where the snow cover is rare on November 1st and
210 shows some variability (Figure 3b-c). The location of the sub-sampled snow forcing however adds snow
211 towards Eastern Eurasia, in locations where the ERA20C snow depth climatology computes a few
212 centimeters of snow. In contrast, snow removal to the west of Russia appears in regions with no to rare
213 snow cover in the ERA20C November 1st climatology. The eastern domain partly covers the Mongolian
214 Plateau region which was shown to exert a strong impact of the wintertime wave fluxes in the
215 stratosphere [White et al., 2017].

216 If not stated otherwise we compute differences between the 5-member ensemble means of the “high
217 snow dipole” and “low snow dipole” in ASF-20C-EXP as well as differences of each ensemble mean
218 relative to the ensemble mean of ASF-20C CTL. We compute significance using a two-sided Student’s
219 t-test.

220 3. Results

221 a. DJF NAO comparison

222 Figure 4a shows the time series of the normalized reconstructed (i.e., based on station data), reanalysed
223 and predicted winter NAO state for the period 1901–2010. Unsurprisingly, the ensemble means of the
224 ASF-20C CTL and ASF-20C EXP forecasts show reduced temporal variance compared to the
225 observation-based NAO datasets. However, single realizations and member spread of the CTL and EXP
226 runs cover the whole range of variability displayed by the observation-based product.

227

228 The correlation between the ERA-20C and CRU NAO index is 0.83, indicating that the EOF approach
229 is a good approximation of the station-based index. It should be noted that the DJF average has a higher
230 correlation between forecasts and reanalyses than the individual monthly correlations within the season
231 (see Supplementary Table S1).

232 The ASF-20C CTL ensemble mean DJF forecast achieves an overall correlation of 0.33 with the CRU
233 NAO reconstruction for the complete time period, with ASF-20C EXP having a nearly identical
234 correlation (0.34). This near-identical correlation is expected given that the land state perturbations
235 across the 21 members are two-sided. Differences between the predicted NAO index of ASF-20C CTL
236 and EXP ensemble means are generally small, with the NAO indices having the same sign during most



237 winters. The correlation between CTL and EXP is 0.8 for the 110-year period. The slightly stronger
238 variability of ASF-20C EXP can partly be attributed to the reduced ensemble size.

239 Contrasting the (initial) high-snow and low-snow composites constructed from the ASF-20C EXP
240 ensemble, we see decadal variability in the difference of winter-mean NAO (Figure 4b&c). The first
241 two decades of the 20th-century are characterized by rather strong negative NAO responses to a strong
242 positive snow dipole. This is followed by two decades spanning the early twentieth century Arctic
243 warming, which shows the opposite response to the multi-step mechanism hypothesized above: A
244 positive snow dipole, as depicted in Figure 4, leads to more positive NAO states compared to a negative
245 snow dipole forcing. After several decades with changing responses to the snow dipole between the two
246 ensembles, eventually the 21st-century starts with a weak negative NAO response to a strong positive
247 snow dipole. Averaged over the whole period, the high-snow ensemble shows a slightly stronger
248 negative NAO response, which is pronounced for extreme NAO states with 51(18) cases of positive
249 (+1 SD) NAO response, 59 (29) cases of negative (-1 SD) NAO response. For 2 SD exceedance, the
250 number of cases is 2 vs 9. Possible reasons for the decadal response to the snow forcing will be
251 considered in the discussion section.

252

253 **b. Regression analysis**

254 Previous studies showed that regressing observed boreal winter zonal-mean temperature and zonal wind
255 anomalies onto an observed Eurasian autumn snow index reveals a significant stratospheric warming
256 and slow-down of the polar vortex starting in November, migrating down towards the tropopause until
257 February. A similar relation between Eurasian snow and the polar stratosphere can be found in the
258 dataset used here.

259 Figure 5 shows a strongly reduced polar vortex for the ERA20C autumn to winter climate anomalies
260 regressed on the November snow dipole index. The zonal wind anomalies in the troposphere highlight
261 a weakened polar jet and an increased subtropical jet, especially in January and February. The
262 concurrent polar stratospheric warming signal moves towards the upper troposphere throughout the
263 winter months, with peak warming at around 100 hPa in February.

264 Spatially, pressure anomalies regressed onto the November snow dipole index reveal that the
265 geographical center of the stratospheric warming is located over the Canadian Arctic (Figure 6).
266 Tropospheric pressure differences highlight a strong ridging over Western Russia and the Ural
267 Mountains in December, which subsequently over the course of winter is shifted more towards
268 Greenland and the Northern North Atlantic region, reflecting a negative NAO-like atmospheric state.
269 This state is further supported by negative DJF SLP anomalies over Southern Europe and the
270 Mediterranean region. Downstream of the Eurasian snow signal, a negative SLP anomaly is found over
271 the Northern North Pacific. The question remains, if these patterns are a result of sampling random co-
272 variability or if the statistical analysis is indeed capturing physical processes.



273 **c. Spatial anomalies in the experiment**

274 In the following paragraphs we investigate the spatial differences in the atmospheric response
275 associated with the high-snow and low-snow ensemble means of ASF-20C EXP, focusing on the initial
276 response in December as well as the average DJF response.

277 Figure 7a&b shows stratospheric geopotential heights anomalies at 10 hPa. In December, a significant
278 negative anomaly formed above Eurasia, corresponding to a polar vortex displacement toward the
279 Eurasian sector and a high over Alaska, as commonly found during stratospheric warming events. Over
280 the course of the winter, this pattern develops into increased geopotential heights over the Arctic with
281 significantly reduced geopotential heights over the extratropics.

282

283 To better understand the wave activity flux into the stratosphere, we investigated the meridional eddy
284 heat flux at 100 hPa, which is proportional to the vertical component of the wave activity flux (Figure
285 7c): it highlights a wave train of circumpolar anomalies in December (hence, following the surface
286 signal forcing in November) with significant positive anomalies over the Ural mountains, eastern North
287 Pacific and the European part of the North Atlantic and negative anomalies over Central and Northern
288 Europe and along the North American Pacific coast. The average DJF response highlights a circumpolar
289 wave-train but shows significant anomalies only for the increased northward heat flux over the northern
290 North Atlantic.

291 Tropospheric circulation anomalies are depicted for geopotential heights at 500hPa in Figure 7e&f. In
292 December, a strong positive anomaly is located over the Barents-Kara Sea sector, with significantly
293 negative anomalies up- and downstream. A second region of positive anomalies emerges at the
294 Canadian Atlantic coast. Both regions match the significant positive anomalies in the 100 hPa heat flux
295 well. The averaged DJF anomalies highlight a negative mid-tropospheric NAO signal with significantly
296 increased geopotential heights above Greenland and Iceland.

297 Sea level pressure anomalies largely mirrors the 500 hPa geopotential height anomalies. The averaged
298 DJF pattern only shows significant increased anomalies over the northern North Atlantic, but still
299 projects onto a meridional pressure gradient characteristic of a negative NAO phase (Fig. 7h). It is
300 important to note, that the absolute difference is rather small compared to interannual SLP variability.
301 Anomalies between the two ensemble-means are around 1 hPa. Even though this number can be
302 assumed to be smaller than in observational datasets due to the ensemble averaging process, it only
303 constitutes ca. 15% of the average 1901–2010 DJF SLP standard deviation over the Euro-Atlantic
304 sector.

305 Due to its large variability, composites of the near-surface temperature are largely non-significant
306 (Figure 7i&j). Yet, in December a clear cooling signal emerges over Central and Eastern Eurasia, as
307 expected from the location of the positive snow anomalies at the time of forecast initialization. At the



308 same time, eastern North America and south-eastern Europe show significant positive temperature
309 anomalies, a result of northward heat advection at the eastern flanks of low-pressure anomalies (Figure
310 7g). Averaged DJF 2m temperatures are significant only for Greenland and Eastern Eurasia, with the
311 cooling over the latter a direct result of the persistence of the anomalously high initial snowpack.

312
313

d. Vertical anomalies in the experiment

314 To get a better understanding on how the different initial conditions impact the vertical distribution of
315 temperature and zonal wind, Figure 8 shows meridional cross-section of the zonal-mean anomalies of
316 zonal wind and temperatures from November to February.

317 While November anomalies (Figure 8) are overall insignificant, a strong snow dipole is associated with
318 an increased polar vortex and cooler stratosphere. In December, zonal wind anomalies are indicative of
319 the tropospheric subtropical jet shifted northward concurrent with a weak Arctic surface warming.
320 Changes are substantial in January, when the stratospheric polar vortex is significantly weakened, with
321 a slight increase in westerlies in the mid-troposphere. The corresponding temperature anomalies show
322 a widespread stratospheric warming and negative anomalies in the lower Arctic troposphere. Eventually
323 in February, the slow-down of westerlies is predicted to reach all the way down from the stratosphere
324 into the troposphere. On the southern flank of these negative zonal wind anomalies, westerly winds are
325 increasing, especially so in the stratosphere. The stratospheric warming signal migrates downwards to
326 the lower stratosphere and tropopause layer. As the warming has migrated down, a stratospheric cooling
327 is forecasted aloft.

328 As a further confirmation, polar cap heights (Supplementary Figure S2) reveal a development of
329 positive anomalies from the surface in December up to the stratosphere in January, migrating back to
330 the troposphere in February.

331

332 Daily evolution of anomalies in the experiment (?)

333 To investigate the temporal evolution and importance of tropospheric anomalies, Figure 9 shows daily
334 mean meridional mean 500 hPa GPH anomalies (high minus low snow dipole ensembles) averaged
335 over 60-70°N. The Hovmöller diagram illustrates the Ural ridge developing only at the end of
336 November going into December and is pre-ceding the development of the North Atlantic ridge, which
337 is the main component of the negative NAO-like feature in our results. It should also be noted that the
338 absence of meaningful anomalies during the first ten days of the composite difference reflects the
339 subtraction of tropospheric anomalies arising from the pre-conditions (since atmospheric initial states
340 are identical among the perturbed ensemble members). The anomalies generated by the end of
341 November do indeed arise from the impact of snow cover differences and snow-atmosphere feedbacks.

342

343 e. Non-linearities in the snow forcing impact



344 Two distinct non-linearities need to be considered. First, a non-linearity in the physical snow feedback:
345 adding a few centimetres of snow in a snow-covered region will not change the radiative and
346 thermodynamic properties of the already snow-covered land surface substantially (due to a saturation
347 effect) but, by contrast, removing a few centimetres of snow might remove the snow layer altogether,
348 changing the albedo and thermodynamics of the surface-atmosphere boundary. This non-linearity may
349 be important for the Rossby wave generation as air flows over the uplifted isentropes above the snow-
350 covered area. The non-linear effect of snow cover saturation and the impact of the relative magnitude
351 of regional surface cooling in our experiments is addressed by Figure 10. In years when the high-minus
352 low snow cover anomalies resulted in a negative NAO anomaly (see Figure 4c for indication of years),
353 the December cooling anomaly over Eastern Eurasia is much stronger than for the opposite case when
354 they resulted in a positive NAO anomaly. Concurrently, the formation of a Ural ridge anomaly is much
355 more pronounced, flanked by troughs up and downstream, with positive eddy heat fluxes into the
356 stratosphere over the Barents-Kara Sea and widespread stratospheric warming. This supports the notion
357 that adding an absolute amount of snow (in either of the two longitudinal domains) is not sufficient for
358 the causal chain to be triggered. Instead, it is a large (in magnitude and extent) relative surface impact
359 of the additional snow that triggers the initial anomalous Rossby wave generation part of the
360 hypothesized causal chain.

361
362 A second non-linearity is the asymmetrical role of the eastern and western domains of the snow dipole.
363 Our subsampling of the ASF-20C EXP simulation allows to estimate the respective roles of these two
364 domains. Interestingly, the difference between the low-snow ensemble mean and the CTL ensemble
365 mean for DJF sea level pressure (Figure 11) reveals a much stronger response to a negative snow dipole
366 (i.e., with high snow depths over Western Russia and low snow depths over Eastern Eurasia) than to
367 the positive snow dipole (i.e., with high snow depths over Eastern Eurasia and low snow depths over
368 Western Russia). In other words, an anomalously negative NAO signal in boreal winter in the high-
369 snow minus low-snow anomalies is mostly a result of an anomalously positive NAO signal in the low-
370 snow ensemble. The negative dipole corresponds to lower snow depths over the eastern domain
371 (Mongolian Plateau and surroundings areas), consistent with lessened wave fluxes into the stratosphere
372 over this region which is the important orographic driver of climatological upward wave fluxes in winter
373 (White et al., 2017). On this note, additional snow right around the Ural Mountains (a negative dipole
374 index) does not enhance the pre-existing role of the Ural mountains in Rossby wave generation by much
375 in our setup.

376 A possible reason for this non-linear behaviour might be found in the importance of the Rossby wave
377 generation via the Eastern Russia cold air dome over the snow-covered area. Based on the snow depth
378 climatology of Eurasia (Figure 3), the negative dipole forcing represents a much more severe disruption
379 to the climatological snow distribution than the positive index forcing is. Removing snow over Eastern



380 Eurasia seems to favour zonal flow more than adding snow is favouring meridional flow. Again, the
381 relative impact of the snow forcing is key in this context. Interestingly, additional snow upstream or
382 just right around the Ural mountains (a negative dipole index) does not seem to enhance the pre-existing
383 role of the Ural mountains in Rossby wave generation by much and we do not find positive the
384 geopotential height anomalies in its vicinity.

385 4. Discussion

386 We used a set of centennial ensemble seasonal forecasts (ASF-20C) and a complementary set with
387 perturbed land initial conditions (ASF-20C-EXP) to address some of the open questions regarding the
388 relationship between Eurasian autumn snow cover and the state of the NAO in the following winter.
389 Subsampling of the latter forecast set according to the initial value (on 1st of November) of a west-east
390 snow dipole over Eurasia (Gastineau et al., 2017; Han and Sun, 2018) allowed us to determine the
391 response over 110 winters.

392 The regression of stratospheric wind and temperature upon the snow dipole in ERA20C over the 1901-
393 2010 period reveals a weakened stratospheric vortex in January and February, following a positive
394 initial snow dipole. The seasonal evolution of the ASF-20C EXP high- minus low-snow anomalies
395 similarly indicates a weakened polar vortex. It also supports the notion of a surface cooling over the
396 Eastern domain anchoring a Ural ridge anomaly on its western flank in December (Figure 7e). This
397 Ural ridge triggers an increased northward heat flux in the lower stratosphere, thereby reducing the
398 polar vortex strength and increasing polar stratospheric temperatures. In January and February, the
399 signal moves downwards into the troposphere where it evolves into a negative NAO anomaly. In
400 general, these results agree with the framework proposed by Cohen et al., (2007) and the experiments
401 with the ECMWF seasonal prediction model by Orsolini et al. (2016). However, it should be highlighted
402 that the absolute ensemble-mean, time-average SLP signal, diagnosed as the conditional composite
403 difference in ASF-20C EXP, is very small, about 1 hPa. As mentioned before, this represents only a
404 small fraction of the interannual SLP variability in the Euro-Atlantic region. Nevertheless, for single
405 realisations of winter forecasts, this impact can be much higher.

406 The role of the Ural ridge in the snow cover \rightarrow NAO causal chain has been discussed and analysed in
407 several recent studies (Peings 2019; Santolaria-Otín et al., 2020). Here we find that the Ural ridge is a
408 pre-condition of predicted negative NAO winters in ASF-20 CTL (Supplementary Figure S3), together
409 with a cold 2m temperature anomaly in Eastern Russia and a cold stratospheric polar vortex displaced
410 over Eurasia, downstream of the Ural ridge. However, these initial conditions are subtracted out in the
411 ASF-20C EXP high- minus low-snow composite difference, and we find that the composite difference
412 indicates a re-enforced Ural ridge (Figure 7e). We find the mid-troposphere Ural ridge is re-enforced
413 only at the end of November going into December, which pre-cedes the formation of a North Atlantic
414 ridge that prevails until February (Figure 9). This result indicates that the snowpack does indeed play a
415 feedback role (see also Orsolini et al., 2016). Thus, we propose that the relation between the Ural ridge



416 and Eurasian snow cover consists of a mutual interaction: the circulation anomaly associated to a pre-
417 existing Ural ridge shovels cold polar air southwards along its eastern flank, allowing for an extensive
418 snow cover to form over Eastern Eurasia (eastern domain of the dipole). In addition to this process
419 (Figure 10c), our analysis reveals that the snow cover anomaly re-enforces the Ural ridge, allowing for
420 increased wave flux into the stratosphere. This particular location of a tropospheric ridge interferes
421 constructively with climatological stationary wave-1 and wave-2 patterns (Garfinkel et al., 2010) and
422 seems to be key for a skilled forecast of the polar winter stratosphere (Portal et al., 2021).

423 Furthermore, the high minus low composite highlights a subpolar North Pacific surface and mi-
424 tropospheric low-pressure anomaly that appears first in December and remain dominant throughout all
425 of DJF (Figures 7e,f,g,i and 11). The generation of this circulation feature was pointed out by previous
426 studies (Orsolini and Kvamstø, 2009; Garfinkel et al., 2010; Garfinkel et al., 2020), and has been
427 attributed to an enhanced vertical propagation of Rossby waves into the stratosphere and horizontal
428 downstream of the cooled Eurasian land mass.

429 Subsampling of the experimental multi-decadal historical forecasts (ASF-20C EXP) highlighted an
430 interdecadal variability and non-stationarity of the snow dipole impact, despite the cancelling out of
431 common boundary forcings such as SST evolution in the composite difference. The configuration of
432 our experiment does not allow to explain this behaviour completely; however, we can address some
433 possible reasons. A potential influence on the decadal variability of the snow cover impact might be the
434 precursory climate system state, promoting or counteracting the tendency for the (perturbed) snow
435 forcing towards a given NAO state.

436 Surprisingly, the positive snow dipole forcing tends to favour a negative NAO signal when the climate
437 system is “tuned” for a positive winter NAO, for example when high Barents-Kara sea ice extent and
438 La Niña SST conditions prevail (Supplementary Figure S4). This supports the idea of a clear and strong
439 snow cover impact when the regional cooling anomaly in Eastern Eurasia is relatively strong and the
440 climate state is preconditioned to a rather positive NAO-like condition. Such snow conditions -
441 corresponding to a positive snow dipole - might amplify the snow feedback in the atmospheric
442 prediction system, tugging the NAO towards a more negative state (while the absolute state might still
443 be positive). This might explain the strong positive anomaly during the early twentieth century Arctic
444 warming in Figure 4c: the period 1920–1940 was characterized by a strong positive mid-tropospheric
445 high anomaly from Northern Europe to East Siberia (Wegmann et al., 2016). We find that the 500 hPa
446 anomalies between high and low snow composites show only a weak to non-existing Ural ridge for the
447 period 1921–1940, when compared to e.g. 1991–2010 (Supplementary Figure S5). On the opposite,
448 adding (removing) snow in Eastern (Western) Eurasia to provide the same response as the pre-existing
449 anomalies favoured by other background conditions, does not seem to have a linear impact. Rather,
450 strong non-linearities seem to occur, which is reasonable given the non-linear thermodynamic and
451 radiative impacts of increased snow cover.



452 On that note, we find that the relative magnitude of regional cooling compared to the existing climate
453 state in our experiments is of crucial importance. In years when the high-minus low snow cover
454 anomalies resulted in a negative NAO, the December cooling anomaly over Eastern Eurasia is much
455 stronger than for the opposite case (Fig. 10). Moreover, we found that a negative snow dipole forcing
456 leading to a positive NAO signal has a much larger relative impact compared to the positive snow dipole
457 resulting in a negative NAO signal. In our experimental setup, snow removal in the eastern domain and
458 snow increase in the western domain allows for a rather zonal circulation in the following months, with
459 no subsequent stratospheric warming signal. Distinct model experiments are needed to understand the
460 atmospheric feedbacks of these configurations better, however it should be kept in mind for future
461 studies using regression or similar statistical tools to infer about the impact of Eurasian snow cover.

462 As such, we find that the main driver for the proposed snow-stratosphere linkage is a large relative
463 impact of the additional snow cover, especially on surface temperatures. Generally, our results further
464 highlight the importance behind the land memory effect discussed by Nakamura et al. (2019), who
465 argue for a delayed impact of snow cover via soil and surface temperatures.

466 Nevertheless, we are limited in analysing the impact of co-variability in the climate system over the
467 span of the 110-year period. Additional experiments are needed to investigate the role of climate state
468 precursors and memory effects influencing the seasonal predictions.

469 **5. Summary and Conclusion**

470 Centennial seasonal ensemble forecasts were used to examine the impact of an increased November
471 Eurasian west-to-east snow cover dipole on the boreal winter climate evolution. We found evidence for
472 the manifestation of a negative NAO signal after a positive November west-to-east snow cover dipole
473 via surface cooling, increased Ural blocking and subsequent stratospheric warming (although evolution
474 toward a positive NAO state was also observed but less frequently, especially for NAO extremes).
475 Including 110-years of natural Earth System variability increases the confidence in the proposed
476 physical mechanisms behind cryospheric drivers of atmospheric variability and decreases the
477 probability of random co-variability between snow cover and DJF NAO. Our results hence support
478 previous hypotheses and statistical studies. The absolute surface impact was found to be small in our
479 experimental setup, with interdecadal variability and ensemble averaging reducing the magnitude of
480 individual events.

481 We found the impact of our snow forcing to be strongest for climate states that will allow the snow
482 forcing to exert a strong surface cooling. Adding additional snow on top of already existing snow-
483 covered and cold surfaces does not linearly strengthen the negative NAO development.

484 Future studies need to address the interplay between different Earth System components in coupled
485 seasonal prediction experiments. How important the background conditions of the climate system are
486 before the initialization of the forecasts needs to be investigated further. Furthermore, allowing more



487 extreme snow forcing (e.g., perturbing initial land states over a longer range than the neighbouring 10
488 years) might result in stronger stratospheric and surface signals.

489

490 **Data availability:**

491 The ERA-20C reanalysis data is publicly available (<https://apps.ecmwf.int/datasets/>). The NAO
492 reconstruction is publicly available at the Climate Research Unit repository
493 (<https://crudata.uea.ac.uk/cru/data/nao/>). The ASF-20C dataset is publicly available at the CEDA
494 Archive (<https://catalogue.ceda.ac.uk/uuid/6e1c3df49f644a0f812818080bed5e45>). The ASF-20C
495 experiment dataset (created by Bart van den Hurk) can be made available on the ECMWF MARS
496 system upon request.

497

498 **Author contribution:**

499 MW and YO designed the study. MW analysed the data. AW and BvH provided the data. GL provided
500 discussion and interpretation of the results. All authors contributed by interpreting the results and
501 writing the paper.

502

503 **Acknowledgements:**

504 The authors thank Daniel Balting for coding advice and Judah Cohen for fruitful discussions. GL and
505 MW received funding through BMBF for the topic "Ocean and Cryosphere under climate change" in
506 the Program "Changing Earth - Sustaining our Future" of the Helmholtz society.

507

508 **Competing Interests:**

509 The authors declare no competing interests.

510 **References**

511 Athanasiadis, P. J., Bellucci, A., Scaife, A. A., Hermanson, L., Materia, S., Sanna, A., Borrelli, A.,
512 MacLachlan, C., and Gualdi, S.: A multisystem view of wintertime nao seasonal predictions,
513 Journal of Climate, 30, 1461–1475, <https://doi.org/10.1175/JCLI-D-16-0153>, 2017.

514 Baker, L. H., Shaffrey, L. C., Sutton, R. T., Weisheimer, A., and Scaife, A. A.: An intercomparison of
515 skill and overconfidence/underconfidence of the wintertime north atlantic oscillation in
516 multimodel seasonal forecasts, Geophysical Research Letters, 45, 7808–7817,
517 <https://doi.org/https://doi.org/10.1029/2018GL078838>, 2018.



- 518 Cohen, J., Barlow, M., Kushner, P. J., and Saito, K.: Stratosphere–troposphere coupling and links with
519 eurasian land surface variability, *Journal of Climate*, 20, 5335–5343,
520 <https://doi.org/10.1175/2007JCLI1725.1>, 2007.
- 521 Cohen, J., and Entekhabi, D.: Eurasian snow cover variability and northern hemisphere climate
522 predictability, *Geophysical Research Letters*, 26, 345–348,
523 <https://doi.org/https://doi.org/10.1029/1998GL900321>, 1999.
- 524 Cohen, J., and Jones, J.: A new index for more accurate winter predictions, *Geophysical Research*
525 *Letters*, 38, <https://doi.org/https://doi.org/10.1029/2011GL049626>, 2011.
- 526 Cohen, J., and Rind, D.: The effect of snow cover on the climate, *Journal of Climate*, 4, 689–706,
527 [https://doi.org/10.1175/1520-0442\(1991\)004<0689:TEOSCO>2.0.CO;2](https://doi.org/10.1175/1520-0442(1991)004<0689:TEOSCO>2.0.CO;2), 1991.
- 528 Cohen, J., Screen, J. A., Furtado, J. C., Barlow, M., Whittleston, D., Coumou, D., Francis, J., Dethloff,
529 K., Entekhabi, D., Overland, J., and Jones, J.: Recent Arctic amplification and extreme mid-
530 latitude weather, *Nature Geoscience*, 7, 627–637, <https://doi.org/10.1038/ngeo2234>, 2014.
- 531 Deser, C., Hurrell, J. W., and Phillips, A. S.: The role of the north atlantic oscillation in european climate
532 projections, *Climate Dynamics*, 49, 3141–3157, <https://doi.org/10.1007/s00382-016-3502-z>,
533 2017.
- 534 Dirmeyer, P. A., Kumar, S., Fennessy, M. J., Altshuler, E. L., DelSole, T., Guo, Z., Cash, B. A., and
535 Straus, D.: Model estimates of land-driven predictability in a changing climate from ccsM4,
536 *Journal of Climate*, 26, 8495–8512, <https://doi.org/10.1175/JCLI-D-13-00029.1>, 2013.
- 537 Douville, H., Peings, Y., and Saint-Martin, D.: Snow-(N)AO relationship revisited over the whole
538 twentieth century, *Geophysical Research Letters*, 44, 569–577,
539 <https://doi.org/https://doi.org/10.1002/2016GL071584>, 2017.
- 540 Dunstone, N., Smith, D., Scaife, A., Hermanson, L., Eade, R., Robinson, N., Andrews, M., and Knight,
541 J.: Skilful predictions of the winter North Atlantic Oscillation one year ahead, *Nature*
542 *Geoscience*, 9, 809–814, <https://doi.org/10.1038/ngeo2824>, 2016.
- 543 Dutra, E., Schär, C., Viterbo, P., and Miranda, P. M. A.: Land-atmosphere coupling associated with
544 snow cover, *Geophysical Research Letters*, 38,
545 <https://doi.org/https://doi.org/10.1029/2011GL048435>, 2011.



- 546 Fletcher, C. G., Hardiman, S. C., Kushner, P. J., and Cohen, J.: The dynamical response to snow cover
547 perturbations in a large ensemble of atmospheric gcm integrations, *Journal of Climate*, 22,
548 1208–1222, <https://doi.org/10.1175/2008JCLI2505.1>, 2009.
- 549 Furtado, J. C., Cohen, J. L., Butler, A. H., Riddle, E. E., and Kumar, A.: Eurasian snow cover variability
550 and links to winter climate in the CMIP5 models, *Climate Dynamics*, 45, 2591–2605,
551 <https://doi.org/10.1007/s00382-015-2494-4>, 2015.
- 552 Furtado, J. C., Cohen, J. L., and Tziperman, E.: The combined influences of autumnal snow and sea ice
553 on Northern Hemisphere winters, *Geophysical Research Letters*, 43, 3478–3485,
554 <https://doi.org/https://doi.org/10.1002/2016GL068108>, 2016.
- 555 Garfinkel, C. I., Hartmann, D. L., and Sassi, F.: Tropospheric precursors of anomalous northern
556 hemisphere stratospheric polar vortices, *Journal of Climate*, 23, 3282–3299,
557 <https://doi.org/10.1175/2010JCLI3010.1>, 2010.
- 558 Garfinkel, C. I., Schwartz, C., White, I. P., and Rao, J.: Predictability of the early winter Arctic
559 oscillation from autumn Eurasian snowcover in subseasonal forecast models, *Climate*
560 *Dynamics*, 55, 961–974, <https://doi.org/10.1007/s00382-020-05305-3>, 2020.
- 561 Gastineau, G., García-Serrano, J., and Frankignoul, C.: The influence of autumnal eurasian snow cover
562 on climate and its link with arctic sea ice cover, *Journal of Climate*, 30, 7599–7619,
563 <https://doi.org/10.1175/JCLI-D-16-0623.1>, 2017.
- 564 Ghatak, D., Frei, A., Gong, G., Stroeve, J., and Robinson, D.: On the emergence of an Arctic
565 amplification signal in terrestrial Arctic snow extent, *Journal of Geophysical Research:*
566 *Atmospheres*, 115, <https://doi.org/https://doi.org/10.1029/2010JD014007>, 2010.
- 567 Gong, G., Entekhabi, D., and Cohen, J.: Modeled northern hemisphere winter climate response to
568 realistic siberian snow anomalies, *Journal of Climate*, 16, 3917–3931,
569 [https://doi.org/10.1175/1520-0442\(2003\)016<3917:MNHWCR>2.0.CO;2](https://doi.org/10.1175/1520-0442(2003)016<3917:MNHWCR>2.0.CO;2), 2003.
- 570 Han, S., and Sun, J.: Impacts of autumnal eurasian snow cover on predominant modes of boreal winter
571 surface air temperature over eurasia, *Journal of Geophysical Research: Atmospheres*, 123,
572 10,076–10,091, <https://doi.org/https://doi.org/10.1029/2018JD028443>, 2018.



- 573 Hardiman, S. C., Kushner, P. J., and Cohen, J.: Investigating the ability of general circulation models
574 to capture the effects of Eurasian snow cover on winter climate, *Journal of Geophysical*
575 *Research: Atmospheres*, 113, [https://doi.org/https://doi.org/10.1029/2008JD010623](https://doi.org/10.1029/2008JD010623), 2008.
- 576 Henderson, G. R., Peings, Y., Furtado, J. C., and Kushner, P. J.: Snow–atmosphere coupling in the
577 Northern Hemisphere, *Nature Climate Change*, 8, 954–963, [https://doi.org/10.1038/s41558-](https://doi.org/10.1038/s41558-018-0295-6)
578 018-0295-6, 2018.
- 579 Hurrell, J. W., and Deser, C.: North atlantic climate variability: The role of the north atlantic oscillation,
580 *Journal of Marine Systems*, 79, 231–244, <https://doi.org/10.1016/j.jmarsys.2009.11.002>, 2010.
- 581 Kang, D., Lee, M.-I., Im, J., Kim, D., Kim, H.-M., Kang, H.-S., Schubert, S. D., Arribas, A., and
582 MacLachlan, C.: Prediction of the Arctic Oscillation in boreal winter by dynamical seasonal
583 forecasting systems, *Geophysical Research Letters*, 41, 3577–3585,
584 [https://doi.org/https://doi.org/10.1002/2014GL060011](https://doi.org/10.1002/2014GL060011), 2014.
- 585 Kretschmer, M., Coumou, D., Agel, L., Barlow, M., Tziperman, E., and Cohen, J.: More-persistent
586 weak stratospheric polar vortex states linked to cold extremes, *Bulletin of the American*
587 *Meteorological Society*, 99, 49–60. <https://doi.org/10.1175/BAMS-D-16-0259.1>, 2018.
- 588 Li, F., Orsolini, Y. J., Keenlyside, N., Shen, M.-L., Counillon, F., and Wang, Y. G.: Impact of snow
589 initialization in subseasonal-to-seasonal winter forecasts with the norwegian climate prediction
590 model, *Journal of Geophysical Research: Atmospheres*, 124, 10033–10048,
591 [https://doi.org/https://doi.org/10.1029/2019JD030903](https://doi.org/10.1029/2019JD030903), 2019.
- 592 Molteni, F., Stockdale, T., Alonso-Balmaseda, M., Balsamo, G., Buizza, R., Ferranti, L., Magnusson,
593 L., Mogensen, K., Palmer, T. N., and Vitart, F.: The new ECMWF seasonal forecast system
594 (System 4). ECMWF Technical Memorandum #656, 2011.
- 595 Moore, G. W. K., and Renfrew, I. A.: Cold European winters: Interplay between the NAO and the East
596 Atlantic mode, *Atmospheric Science Letters*, 13, 1–8.
597 [https://doi.org/https://doi.org/10.1002/asl.356](https://doi.org/10.1002/asl.356), 2012.
- 598 Nakamura, T., Yamazaki, K., Sato, T., and Ukita, J.: Memory effects of Eurasian land processes cause
599 enhanced cooling in response to sea ice loss, *Nature Communications*, 10, 5111.
600 <https://doi.org/10.1038/s41467-019-13124-2>, 2019.



- 601 O'Reilly, C. H., Heatley, J., MacLeod, D., Weisheimer, A., Palmer, T. N., Schaller, N., and Woollings,
602 T.: Variability in seasonal forecast skill of Northern Hemisphere winters over the twentieth
603 century, *Geophysical Research Letters*, 44, 5729–5738,
604 <https://doi.org/https://doi.org/10.1002/2017GL073736>, 2017.
- 605 O'Reilly, C. H., Weisheimer, A., MacLeod, D., Befort, D. J., and Palmer, T.: Assessing the robustness
606 of multidecadal variability in Northern Hemisphere wintertime seasonal forecast skill,
607 *Quarterly Journal of the Royal Meteorological Society*, 146, 4055–4066,
608 <https://doi.org/https://doi.org/10.1002/qj.3890>, 2020.
- 609 Orsolini, Y. J., Senan, R., Balsamo, G., Doblas-Reyes, F. J., Vitart, F., Weisheimer, A., Carrasco, A.,
610 and Benestad, R. E.: Impact of snow initialization on sub-seasonal forecasts, *Climate*
611 *Dynamics*, 41, 1969–1982, <https://doi.org/10.1007/s00382-013-1782-0>, 2013.
- 612 Orsolini, Y. J., Senan, R., Vitart, F., Balsamo, G., Weisheimer, A., and Doblas-Reyes, F. J.: Influence
613 of the Eurasian snow on the negative North Atlantic Oscillation in subseasonal forecasts of the
614 cold winter 2009/2010, *Climate Dynamics*, 47, 1325–1334, [https://doi.org/10.1007/s00382-](https://doi.org/10.1007/s00382-015-2903-8)
615 [015-2903-8](https://doi.org/10.1007/s00382-015-2903-8), 2016.
- 616 Parker, T., Woollings, T., Weisheimer, A., O'Reilly, C., Baker, L., and Shaffrey, L.: Seasonal
617 predictability of the winter north atlantic oscillation from a jet stream perspective, *Geophysical*
618 *Research Letters*, 46, 10159–10167, <https://doi.org/https://doi.org/10.1029/2019GL084402>,
619 2019.
- 620 Peings, Y.: Ural blocking as a driver of early-winter stratospheric warmings, *Geophysical Research*
621 *Letters*, 46, 5460–5468, <https://doi.org/https://doi.org/10.1029/2019GL082097>, 2019.
- 622 Peings, Y., Brun, E., Mauvais, V., and Douville, H.: How stationary is the relationship between Siberian
623 snow and Arctic Oscillation over the 20th century?, *Geophysical Research Letters*, 40, 183–
624 188, <https://doi.org/https://doi.org/10.1029/2012GL054083>, 2013.
- 625 Peings, Y., Douville, H., Colin, J., Martin, D. S., and MagnUSDottir, G.: Snow–(N)ao teleconnection
626 and its modulation by the quasi-biennial oscillation, *Journal of Climate*, 30, 10211–10235,
627 <https://doi.org/10.1175/JCLI-D-17-0041.1>, 2017.



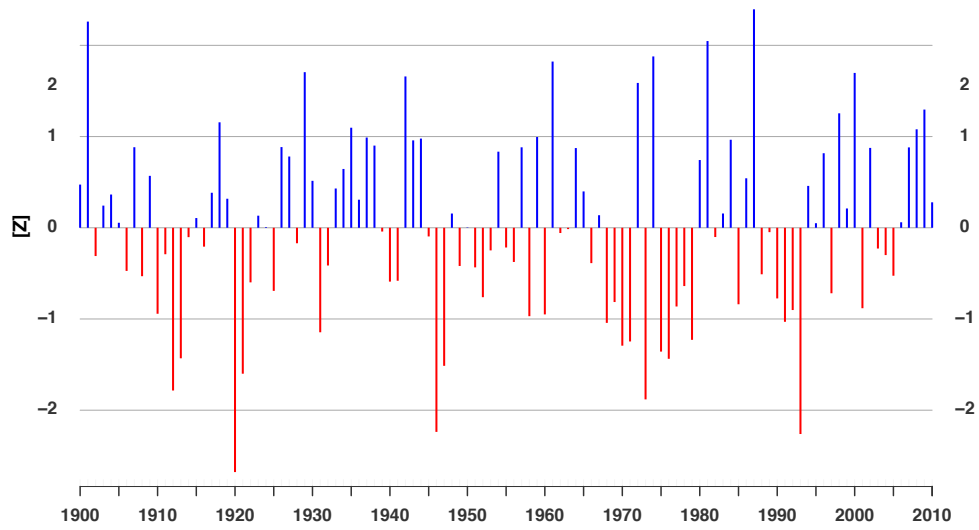
- 628 Peings, Y., Saint-Martin, D., and Douville, H.: A numerical sensitivity study of the influence of siberian
629 snow on the northern annular mode, *Journal of Climate*, 25, 592–607,
630 <https://doi.org/10.1175/JCLI-D-11-00038.1>, 2012.
- 631 Portal, A., Ruggieri, P., Palmeiro, F. M., García-Serrano, J., Domeisen, D. I., & Gualdi, S.: Seasonal
632 prediction of the boreal winter stratosphere, *Climate Dynamics*, 1-22, 2021.
- 633 Santolaria-Otín, M., García-Serrano, J., Ménégoz, M., and Bech, J.: On the observed connection
634 between Arctic sea ice and Eurasian snow in relation to the winter North Atlantic Oscillation,
635 *Environmental Research Letters*, 15, 124010, <https://doi.org/10.1088/1748-9326/abad57>, 2021.
- 636 Santolaria-Otín, M., and Zolina, O.: Evaluation of snow cover and snow water equivalent in the
637 continental Arctic in CMIP5 models, *Climate Dynamics*, 55, 2993–3016,
638 <https://doi.org/10.1007/s00382-020-05434-9>, 2020.
- 639 Scaife, A. A., Arribas, A., Blockley, E., Brookshaw, A., Clark, R. T., Dunstone, N., Eade, R., Fereday,
640 D., Folland, C. K., Gordon, M., Hermanson, L., Knight, J. R., Lea, D. J., MacLachlan, C.,
641 Maidens, A., Martin, M., Peterson, A. K., Smith, D., Vellinga, M., Wallace, E., Waters, J. and
642 Williams, A.: Skillful long-range prediction of European and North American winters,
643 *Geophysical Research Letters*, 41, 2514–2519,
644 <https://doi.org/https://doi.org/10.1002/2014GL059637>, 2014.
- 645 Scaife, A. A., Karpechko, A. Y., Baldwin, M. P., Brookshaw, A., Butler, A. H., Eade, R., Gordon, M.,
646 MacLachlan, C., Martin, N., Dunstone, N., and Smith, D.: Seasonal winter forecasts and the
647 stratosphere, *Atmospheric Science Letters*, 17, 51–56,
648 <https://doi.org/https://doi.org/10.1002/asl.598>, 2016.
- 649 Smith, D. M., Scaife, A. A., Eade, R., and Knight, J. R.: Seasonal to decadal prediction of the winter
650 North Atlantic Oscillation: Emerging capability and future prospects, *Quarterly Journal of the*
651 *Royal Meteorological Society*, 142, 611–617, <https://doi.org/https://doi.org/10.1002/qj.2479>,
652 2016.
- 653 Song, L., & Wu, R., 2019: Intraseasonal snow cover variations over western Siberia and associated
654 atmospheric processes, *Journal of Geophysical Research: Atmospheres*, 124, 8994–



- 655 9010.Thackeray, C. W., Derksen, C., Fletcher, C. G., and Hall, A.: Snow and climate:
656 Feedbacks, drivers, and indices of change, *Current Climate Change Reports*, 5, 322–333,
657 <https://doi.org/10.1007/s40641-019-00143-w>, 2019.
- 658 Thompson, D. W. J., and Wallace, J. M.: The Arctic oscillation signature in the wintertime geopotential
659 height and temperature fields, *Geophysical Research Letters*, 25, 1297–1300,
660 <https://doi.org/10.1029/98GL00950> , 1998.
- 661 Tian, B., and Fan, K.: A skillful prediction model for winter nao based on atlantic sea surface
662 temperature and eurasian snow cover, *Weather and Forecasting*, 30, 197–205,
663 <https://doi.org/10.1175/WAF-D-14-00100.1>, 2015.
- 664 Tyrrell, N. L., Karpechko, A. Y., and Räisänen, P.: The influence of eurasian snow extent on the
665 northern extratropical stratosphere in a qbo resolving model, *Journal of Geophysical Research:
666 Atmospheres*, 123, 315–328, <https://doi.org/https://doi.org/10.1002/2017JD027378>, 2018.
- 667 Tyrrell, N. L., Karpechko, A. Y., Uotila, P., and Vihma, T.: Atmospheric circulation response to
668 anomalous siberian forcing in october 2016 and its long-range predictability, *Geophysical
669 Research Letters*, 46, 2800–2810, <https://doi.org/https://doi.org/10.1029/2018GL081580> ,
670 2019.
- 671 van den Hurk, B., Kim, H., Krinner, G., Seneviratne, S. I., Derksen, C., Oki, T., Douville, H., Colin, J.,
672 Ducharne, A., Cheruy, F., Viovy, N., Puma, M. J., Wada, Y., Li, W., Jia, B., Alessandri, A.,
673 Lawrence, D. M., Weedon, G. P., Ellis, R., Hagemann, S., Mao, J., Flanner, M. G., Zampieri,
674 M., Materia, S., Law, R. M., and Sheffield, J.: Ls3mip (V1. 0) contribution to cmip6: The land
675 surface, snow and soil moisture model intercomparison project – aims, setup and expected
676 outcome, *Geoscientific Model Development*, 9, 2809–2832, [https://doi.org/10.5194/gmd-9-
677 2809-2016](https://doi.org/10.5194/gmd-9-2809-2016) , 2016.
- 678 Vavrus, S.: The role of terrestrial snow cover in the climate system, *Climate Dynamics*, 29, 73–88,
679 <https://doi.org/10.1007/s00382-007-0226-0>, 2007.
- 680 Wang, L., Ting, M., and Kushner, P. J.: A robust empirical seasonal prediction of winter NAO and
681 surface climate, *Scientific Reports*, 7, 279, <https://doi.org/10.1038/s41598-017-00353-y> , 2017.

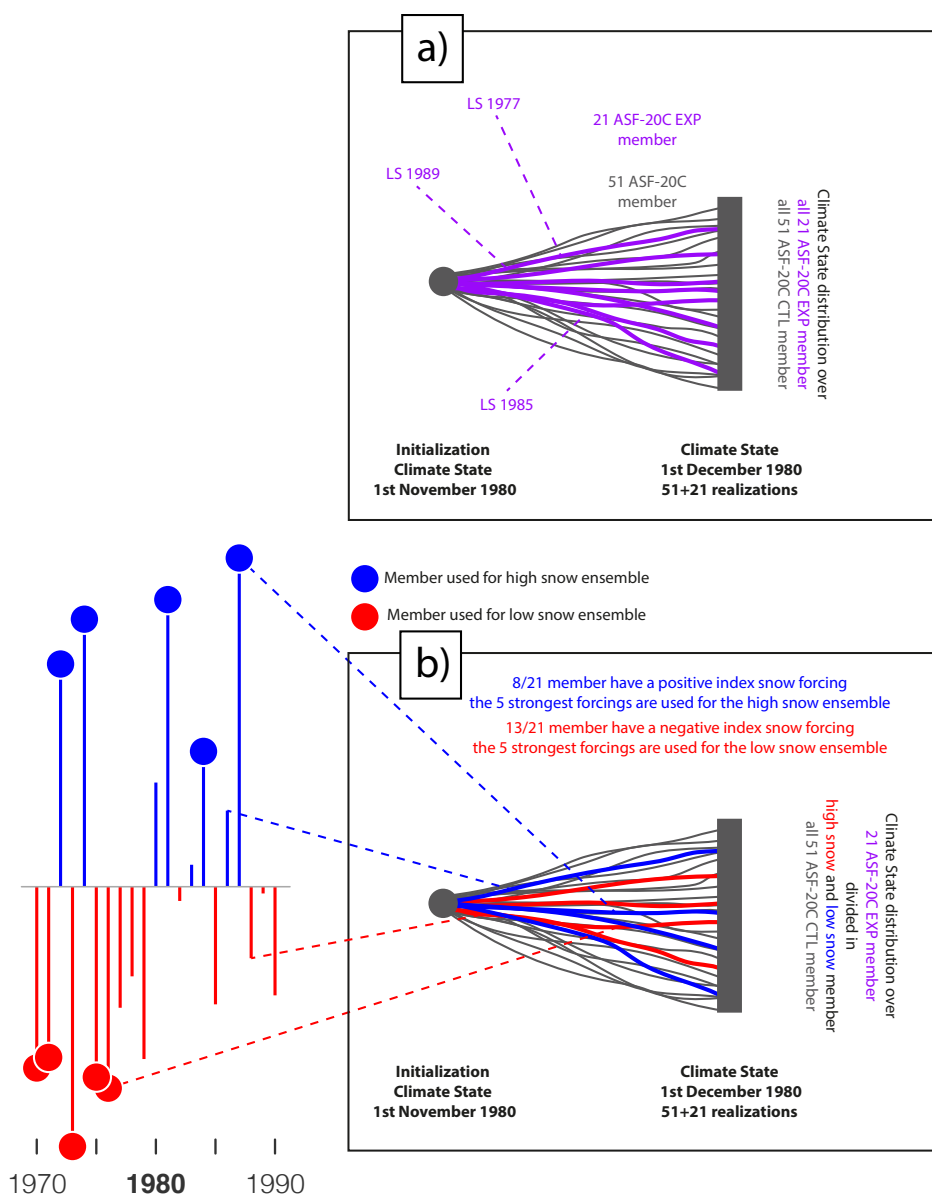


- 682 Wanner, H., Brönnimann, S., Casty, C., Gyalistras, D., Luterbacher, J., Schmutz, C., Stephenson, D.
683 B., and Xoplaki, E.: North atlantic oscillation – concepts and studies, *Surveys in Geophysics*,
684 22, 321–381, <https://doi.org/10.1023/A:1014217317898>, 2001.
- 685 Wegmann, M., Orsolini, Y., Vázquez, M., Gimeno, L., Nieto, R., Bulygina, O., Jaiser, R., Handorf, D.,
686 Rinke, A., Dethloff, K., Sterin, A., and Brönnimann, S.: Arctic moisture source for Eurasian
687 snow cover variations in autumn, *Environmental Research Letters*, 10, 054015,
688 <https://doi.org/10.1088/1748-9326/10/5/054015>, 2015.
- 689 Wegmann, M., Rohrer, M., Santolaria-Otín, M., and Lohmann, G.: Eurasian autumn snow link to winter
690 North Atlantic Oscillation is strongest for Arctic warming periods, *Earth System Dynamics*,
691 11, 509–524, <https://doi.org/https://doi.org/10.5194/esd-11-509-2020>, 2020.
- 692 Weisheimer, A., Befort, D. J., MacLeod, D., Palmer, T., O’Reilly, C., and Strømmen, K.: Seasonal
693 forecasts of the twentieth century, *Bulletin of the American Meteorological Society*, 101,
694 E1413–E1426, <https://doi.org/10.1175/BAMS-D-19-0019.1>, 2020.
- 695 Weisheimer, A., Decremmer, D., MacLeod, D., O’Reilly, C., Stockdale, T. N., Johnson, S., and Palmer,
696 T. N.: How confident are predictability estimates of the winter North Atlantic Oscillation?,
697 *Quarterly Journal of the Royal Meteorological Society*, 145, 140–159,
698 <https://doi.org/https://doi.org/10.1002/qj.3446>, 2019.
- 699 Weisheimer, A., Schaller, N., O’Reilly, C., MacLeod, D. A., and Palmer, T.: Atmospheric seasonal
700 forecasts of the twentieth century: Multi-decadal variability in predictive skill of the winter
701 North Atlantic Oscillation (Nao) and their potential value for extreme event attribution,
702 *Quarterly Journal of the Royal Meteorological Society*, 143, 917–926,
703 <https://doi.org/https://doi.org/10.1002/qj.2976>, 2017.
- 704 White, R. H., Battisti, D. S., & Roe, G. H.: Mongolian Mountains Matter Most: Impacts of the Latitude
705 and Height of Asian Orography on Pacific Wintertime Atmospheric Circulation, *Journal of*
706 *Climate*, 30, 4065–4082, 2017.
- 707 Zhang, R., Sun, C., Zhang, R., Li, W., and Zuo, J.: Role of Eurasian snow cover in linking winter-spring
708 Eurasian coldness to the autumn arctic sea ice retreat, *Journal of Geophysical Research:*
709 *Atmospheres*, 124, 9205–9221, <https://doi.org/https://doi.org/10.1029/2019JD030339>, 2019.



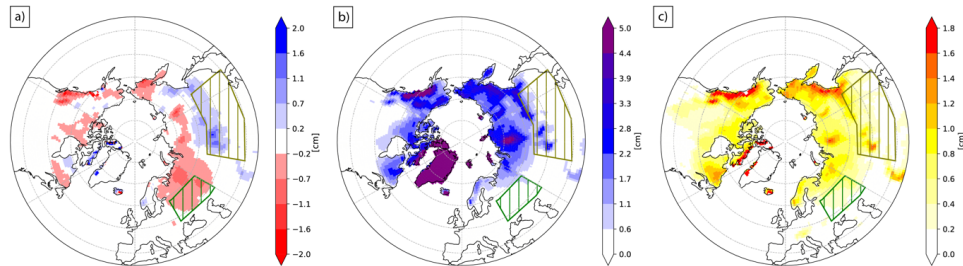
710

711 *Figure 1: Normalized 1st of November Eurasian snow dipole index for the period 1900–2010 as derived*
712 *from ERA20C.*

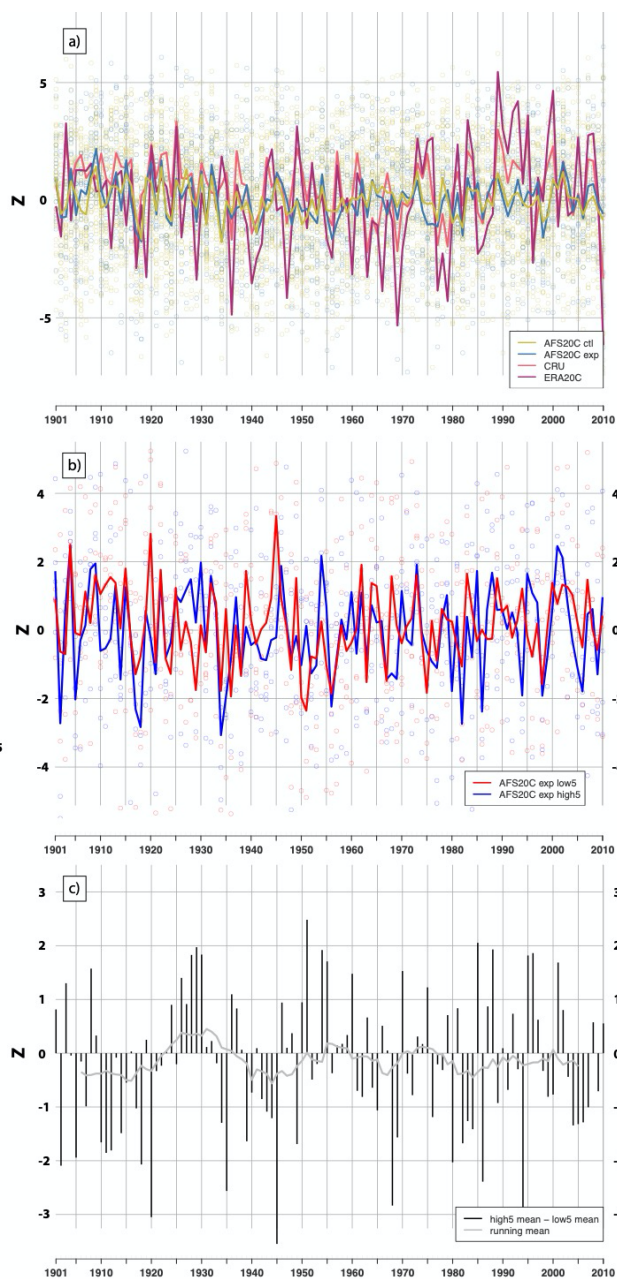


713

714 *Figure 2: As example, the schematic for a) the 1980 1st of November ASF-20C EXP initialization and*
 715 *the consequent sampling of the 21 ensemble members into the high and low snow dipole ensembles. For*
 716 *the 1st of November initialization, ASF-20C EXP members are initialized by land surface conditions of*
 717 *the 21 surrounding 1st of November dates, in this case 1970–1990, b) Out of these 21 members, we*
 718 *sample individual members based on their ranking in the snow index. The five members with the most*
 719 *positive snow index constitute the high snow ensemble and vice versa for the low snow ensemble.*



720
721 *Figure 3: a) Average (1900–2010) 1st of November snow depth difference between the high-snow and*
722 *low-snow ensemble. b) Average (1900–2010) 1st of November snow depth. c) Average (1900–2010) 1st*
723 *of November snow depth standard deviation. Hatched in green (olive) is the western (eastern) domain*
724 *of the snow index. All 3 plots are based on ERA20C.*
725

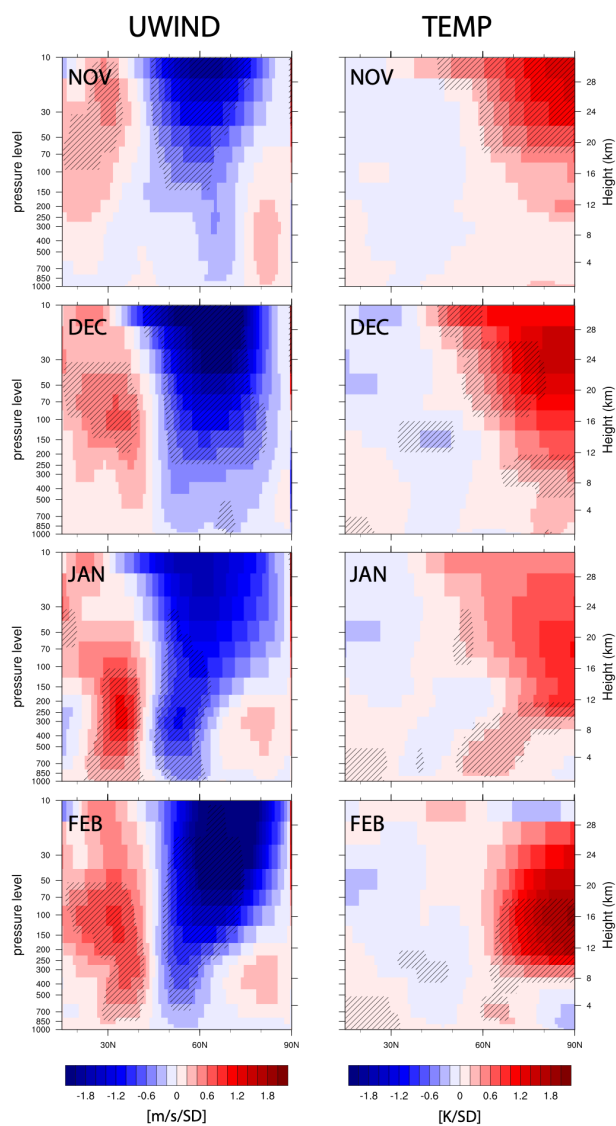


726

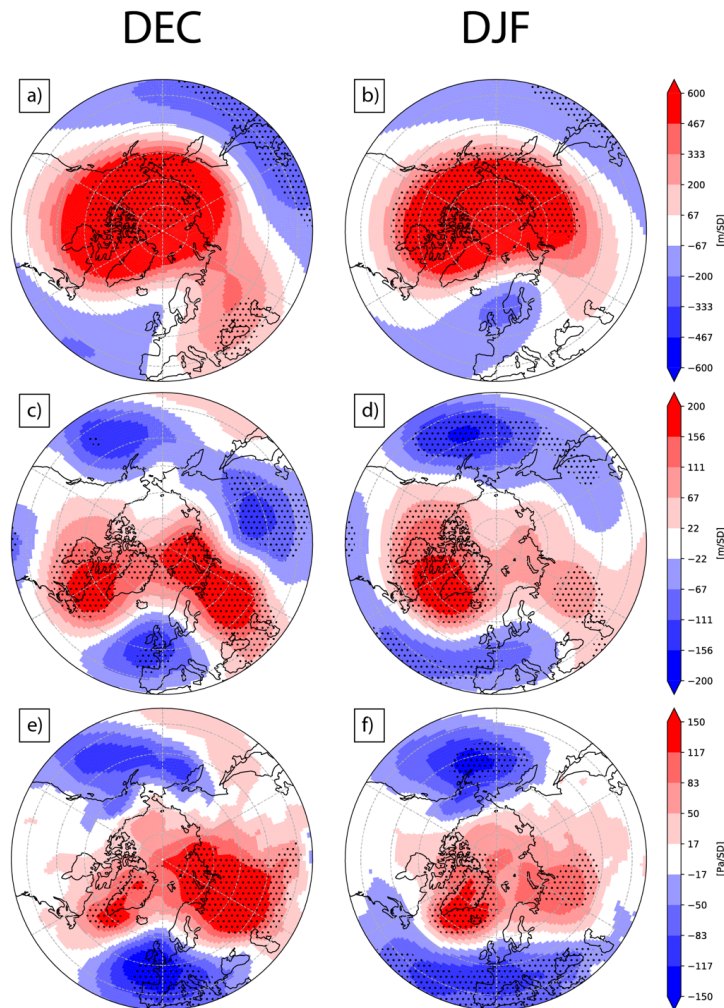
727 *Figure 4: Time series of DJF NAO for the period 1901–2010. a) Normalized DJF NAO index in the*
728 *CRU station-based reconstruction, ERA20C EOF-based index, ASF-20C CTL and ASF-20C EXP EOF-*
729 *based index. Hollow points represent individual member, solid lines represent ensemble means or*
730 *observational products. b) 5-member DJF NAO forecasts for the high- and low-snow members within*
731 *ASF-20C EXP. Hollow points represent individual member, solid lines represent ensemble means. c)*
732 *NAO DJF state difference and its 11-year running mean between the ASF-20C EXP high- and low-*



733 snow ensemble mean in panel b (51(18) cases of positive (+1 SD) NAO response, 59 (29) cases of
734 negative (-1 SD) NAO response). For 2 SD exceedance, the number of cases is 2 vs 9.

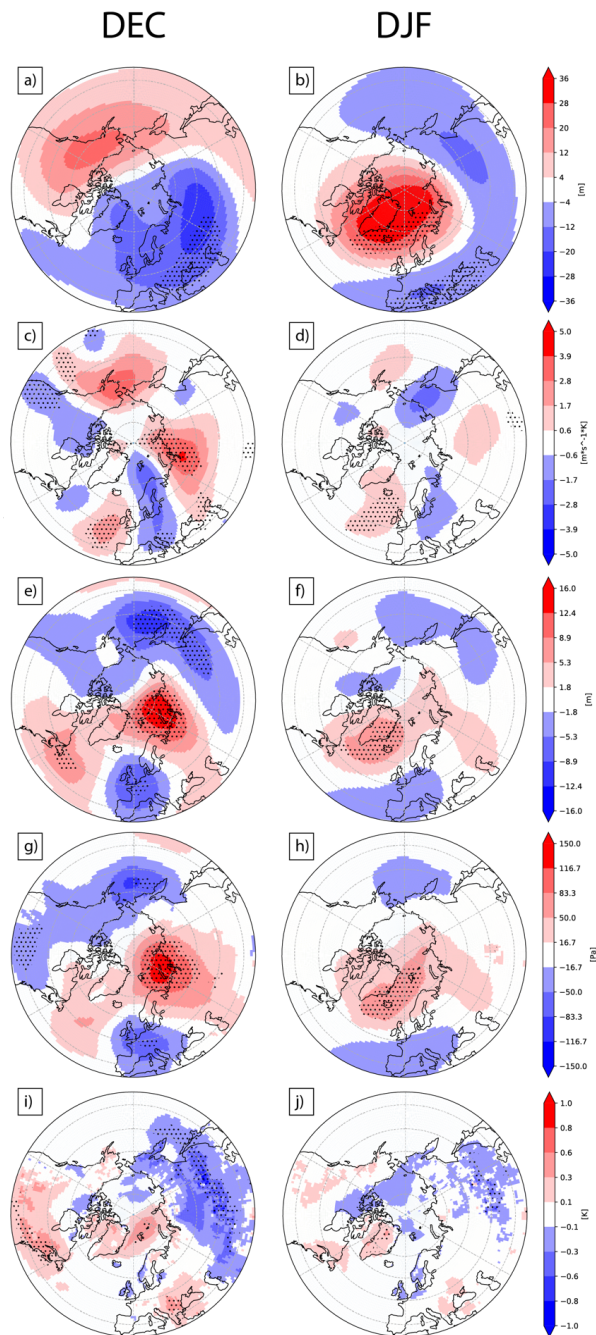


735
736 Figure 5: Zonal-mean meridional cross-section of ERA20C anomalies in temperature and zonal wind
737 regressed onto the snow dipole index in November from ERA20C covering 1901–2010 for November,
738 December, January and February. Shading indicates 95% significance level.

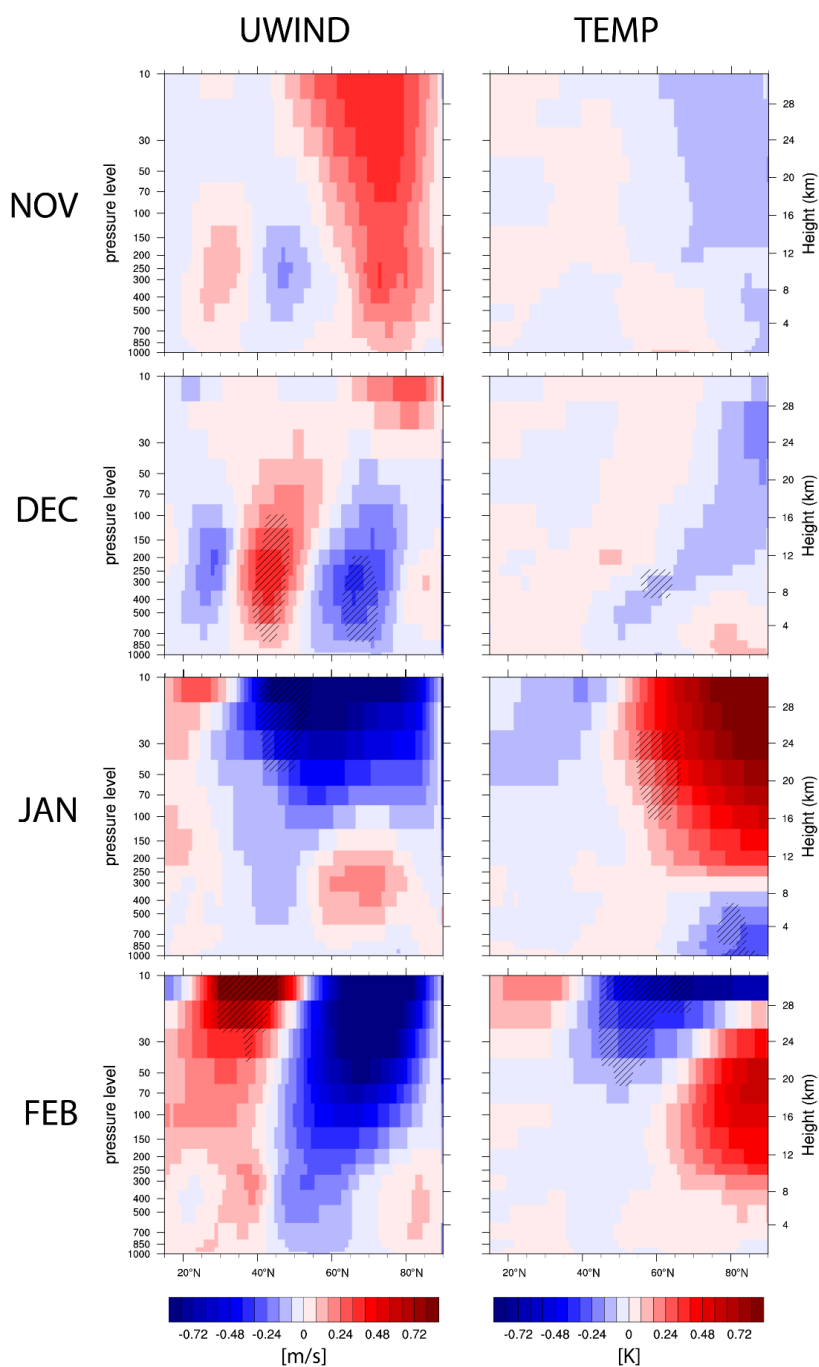


739

740 *Figure 6: ERA20C anomalies of a&b)10 hPa geopotential heighth, c&d) 500 hPa geopotential heights*
741 *and e&f) Sea Level Pressure regressed onto the snow dipole index in November from ERA20C covering*
742 *1901–2010 for December and DJF mean. Shading indicates 95% significance level.*

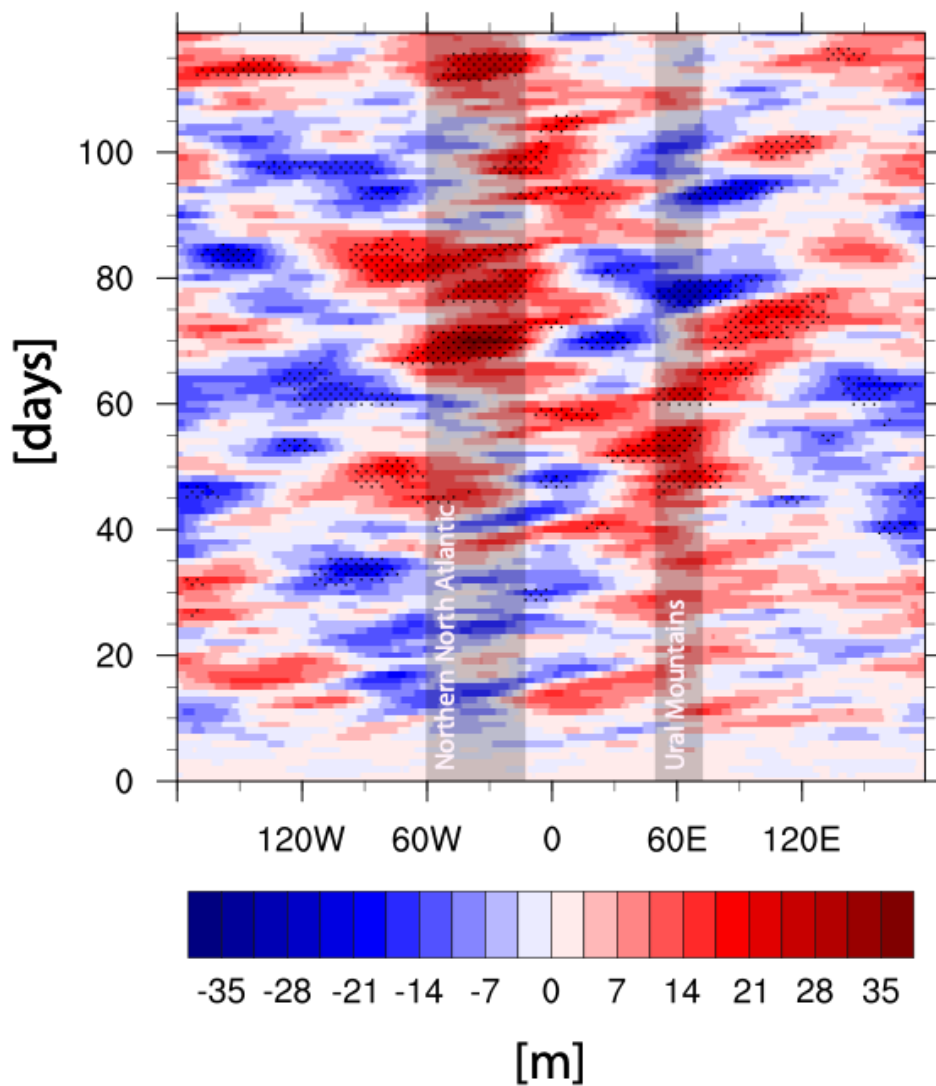


743
 744 *Figure 7: Averaged anomalies 1901-2010 between high-snow and low-snow ASF-20C EXP ensemble*
 745 *means for December (a,c,e,g,i), and DJF (b,d,f,i,k): a&b) 10 hPa geopotential heights, c&d) 100 hPa*
 746 *meridional eddy heat flux, e&f) 500 hPa geopotential heights, g&h) sea level pressure and i&j) 2m*
 747 *temperature. Stippled areas represent 90% significance.*



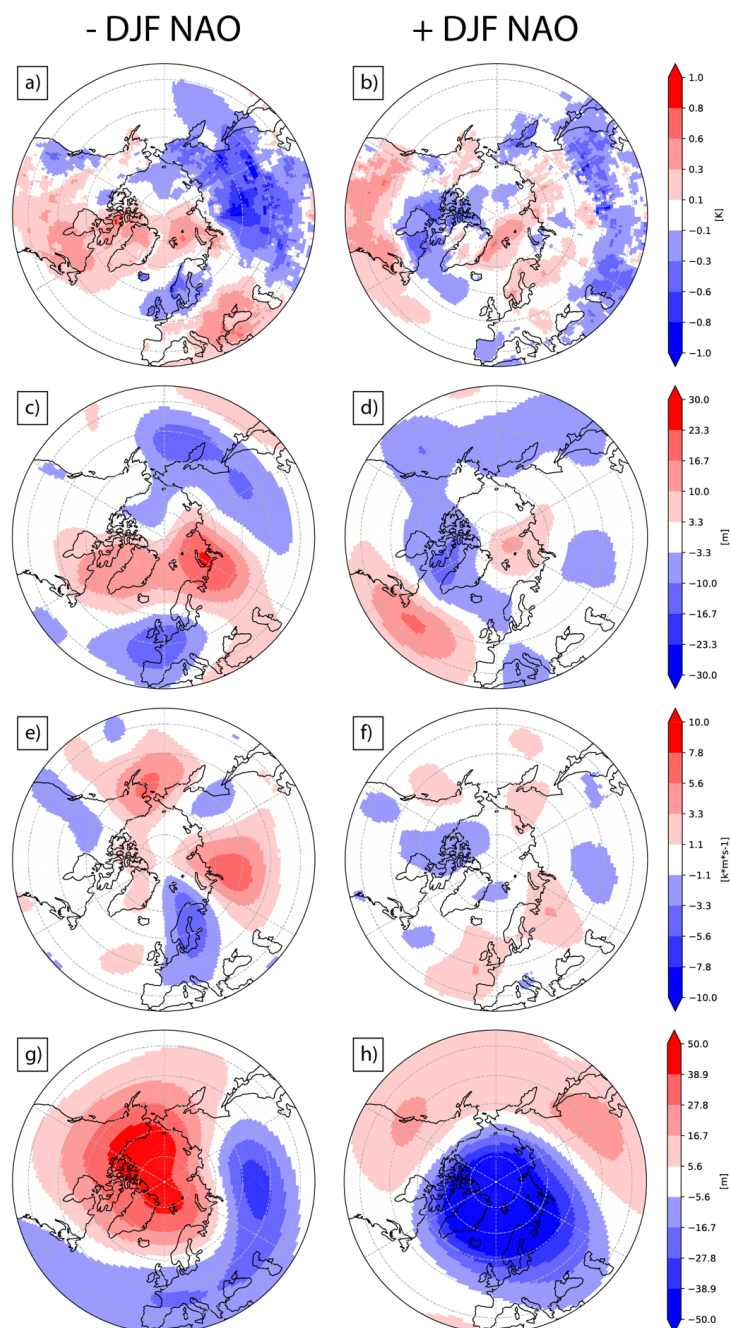
748

749 *Figure 8: Zonal-mean cross-section of left) zonal wind anomalies and right) temperature anomalies for*
750 *the period 1901-2010 between high-snow and low-snow ASF-20C EXP ensemble means. Shading*
751 *indicates 90% significance level.*



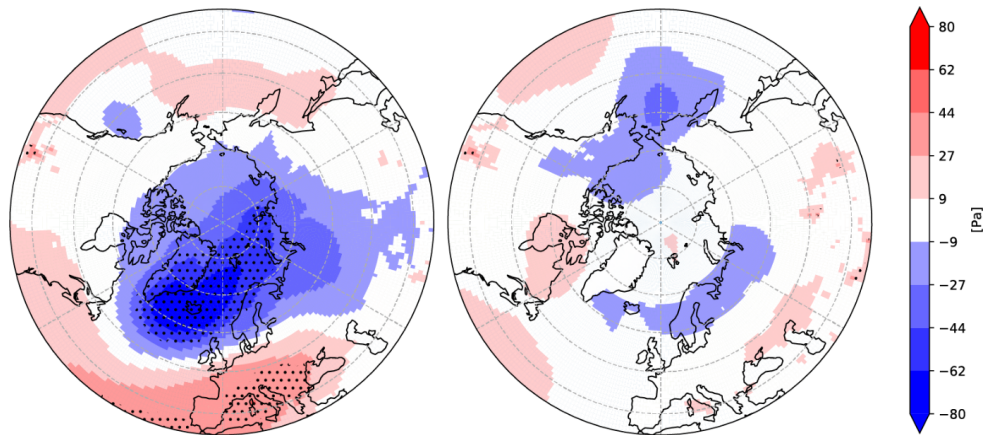
752

753 *Figure 9: Hovmöller diagram of daily mean predicted 500 hPa geopotential height anomalies for the*
754 *period 1901-2010 averaged for the latitude band 60°-70°N difference between high-snow and low-snow*
755 *ASF-20C EXP ensemble means. Stippled areas represent 90% significance. Days from NOV 1st are*
756 *indicated on y-axis.*



757

758 *Figure 10: Climate anomaly composites of predicted December fields after which a positive snow dipole*
759 *forcing resulted in a negative DJF NAO signal (a,c,e,g) or a positive DJF NAO signal (b,d,f,i)(selection*
760 *of years based on Figure 4c): a&b) 2m temperature, c&d) 500 hPa geopotential heights, e&f) 100hPa*
761 *meridional eddy temperature flux, g&h) 10 hPa geopotential heights. Anomalies are based on ASF-*
762 *20C EXP high minus low snow ensemble mean data.*



763

764 *Figure 11: Mean sea level pressure [unit] DJF anomalies for the period 1901-2010 between a) low-*
765 *snow ASF-20C EXP ensemble mean and ASF-20C CTL ensemble mean (subsamped from 21 CTL*
766 *members) and b) high-snow ASF-20C EXP ensemble mean and ASF-20C CTL ensemble mean*
767 *(subsamped from 21 CTL members). Stippled areas represent 90% significance.*

768